4th Micro and Nano Flows Conference
UCL, London, UK, 7-10 September 2014

A numerical study of bubble growing during saturated and sub-cooled flow boiling in micro channels

Qingming LIU, Björn PALM*
*Corresponding author: Tel: +46 (0)8 790 7453; Fax: +46 (0)8 20 41 61, Email: Bjorn.Palm@energy.kth.se
Department of Energy Technology, Royal Institute of Technology KTH
10044 Stockholm, SWEDEN

Abstract

A CFD study of bubbles growing in a mini-channel with a diameter of 0.64 mm has been done. Coupled level set and volume of fluid (CLSVOF) method is applied to capture the two phase interface. Geo-reconstruct method is used to re-construct the two-phase interface. A constant velocity inlet boundary with mass flux 335 kg/m^2s and a heated boundary wall with constant heat flux ($10kW/m^2$) is applied. Both saturated and sub-cooled inlet condition are studied. The growth of bubbles and the transition of flow regime differs each other under these two conditions. Sub-cooling significantly lowers the bubble growth rate. However, it does not affect the heat transfer coefficient at the same level due to its complicated heat transfer mechanism.

Key words:

CFD, heat transfer, boiling, bubbles, evaporation, multi-phase flow, micro-channel

1 Introduction

The study of micro-channels has become an emerging research topic only very recently. The advancements of MEMS (micro-electro - mechanical systems), fuel cells, cooling of micro-electronic chips, and also, compact heat exchangers lead to an increasing demand for the understanding of heat transfer in micro-channels.

While single phase flow in micro-channels has been comprehensively studied during the past three decades, the study of flow boiling is relatively rare and there are still many unsolved questions. Additionally, the mechanisms are much more complicated than in single phase flow due to the many reasons: interface phenomena, turbulence induced by bubble generation and moving.

The presented study of two-phase flow in macro-channels has indicated that there are several kinds of flow patterns, of which the most important are: bubbly flow, slug flow, annular flow and mist flow. However, the study of the flow pattern in micro channel (Thome and Collier 1994; Owhaib 2009) has shown that two new flow patterns, confined bubbly flow and elongated bubbly/slug flow, appear besides the conventional four flow patterns (Figure 1- right). These new flow patterns and the downstream annular flow play an important role in the heat transfer process.

In order to investigate these new flow regimes, Mukejee and Kandlikar simulated the growth of a confined bubble in a rectangle micro channel(Mukherjee and Kandlikar 2005). Special attention had also been put on elongated bubbles(Agostini, Revellin et al. 2008) as an experiment was implemented to study the velocity of elongated bubble in diabatic micro channels and predicative

model was proposed. Furthermore, the collision process of elongated bubbles in micro channels, though without heat transfer(Revellin, Agostini et al. 2008). Regarding numerical studies, Liu and et al(Liu, Palm et al. 2012) examined the confined bubbles heat transfer and effect of contact angle. Magnini and et al(Magnini, Pulvirenti et al. 2013) developed a height algorithm and investigated the leading elongated bubble.

In spite of these efforts, the transition between the bubbly flow and confined bubbles has not been comprehensive studied, the effects of inlet conditions such as sub-cooling is also of interest and believed to play an key role.

2 Numerical model

2.1 Coupling level set and volume of fluid method (CLSVOF)

The governing equations of CLSVOF method are summarized as follows:

$$\frac{\partial \rho}{\partial t} + \nabla \cdot (\rho \boldsymbol{u}) = 0 \; ; \tag{1}$$

$$\rho\left(\frac{\partial \boldsymbol{u}}{\partial t} + \boldsymbol{u} \cdot \boldsymbol{\nabla u}\right) = -\boldsymbol{\nabla} P + \boldsymbol{\nabla}\left(\mu(\boldsymbol{\nabla} \cdot \boldsymbol{u} + \boldsymbol{\nabla} \cdot \boldsymbol{u}^T)\right) + \rho g + \boldsymbol{F_\sigma} \tag{2}$$

$$\rho C_p\left(\frac{\partial \boldsymbol{T}}{\partial t} + \boldsymbol{u} \cdot \boldsymbol{\nabla T}\right) = \boldsymbol{\Phi} + \boldsymbol{\nabla} \cdot (k \boldsymbol{\nabla} T) \tag{3}$$

$$\frac{\partial \alpha}{\partial t} + \boldsymbol{u} \nabla \alpha = 0 \; ; \tag{4}$$

$$\frac{\partial \phi}{\partial t} + \boldsymbol{u} \nabla \phi = 0 \; ; \tag{5}$$

They are the continuity equation (equation 1), the momentum equation (equation 2), the energy equation (equation 3), the volume fraction (equation 4), and level-set equation respectively.

All the physical properties, such as density, viscosity, thermal conductivity, are the average value of all the phases in the cell and have the following form:

$$\Phi = \sum_{1}^{n} \Phi_i \alpha_i \tag{6}$$

The α in equation 4 is the volume fraction of the primary phase (gas in this paper) in each computational volume

$$\alpha(x,t) = \begin{matrix} 1 \; x \in primary\ phase \\ (0,1) \quad if \; x \in interface\ \Gamma \\ 0 \; x \in secondary\ phase \end{matrix} \tag{7}$$

The level-set function ϕ is a signed distance, to the interface. Accordingly, the interface is the zero level-set.

$$\phi(x,t) = \begin{matrix} + \quad x \in primary\ phase \\ 0 \quad if \; x \in interface\ \Gamma \\ - \quad x \in secondary\ phase \end{matrix} \tag{8}$$

Solve the level set equation to get the curvature and normal to interface

$$\boldsymbol{n} = \frac{\nabla \phi}{|\nabla \phi|} \quad \boldsymbol{k} = \nabla \cdot \frac{\nabla \phi}{|\nabla \phi|} \tag{9}$$

Then get the surface tension force by the following equation

$$\boldsymbol{F_\sigma} = -\sigma \boldsymbol{k} \boldsymbol{\delta}(\phi) \nabla \phi \tag{10}$$

Where

$$\boldsymbol{\delta}(\phi) = \frac{1 - cos(3\pi\phi / 2L_{gr})}{3L_{gr}} \tag{11}$$

Where L_{gr} is the minimum grid spacing.

2.2 Phase change model

The evaporation heat at the interface is calculated by the following equation:

$$q_{e0} = \frac{T_{int} - T_{sat}}{R_{int}} \tag{12}$$

Where T_{int} is the interface temperature and R_{int} is the interfacial resistance defined as:

$$R_{int} = \frac{2-C}{2C}\frac{\sqrt{2\pi R_{gas}}}{{h_e}^2}\frac{{T_{sat}}^{3/2}}{\rho_v} \qquad (13)$$

where C is the evaporation/condensation (or accommodation) coefficient and usually has a value of unit.

The detail of the implementation of this model can be refer to Hardt et al (Hardt and Wondra 2008) and Liu et al (Liu, Palm et al. 2012).

2.3 Computation domain

A micro-channel with a diameter of 0.64 mm and length of 5 mm is studied in this paper. The channel is vertical placed implying a $-Z$ direction gravity vector. Cartesian coordinates are used with hexahedra grid. Two perpendicular symmetry boundaries are defined at the center of the tube so only a quarter of the tube needs to be calculated. This would significantly reduce the computational time.

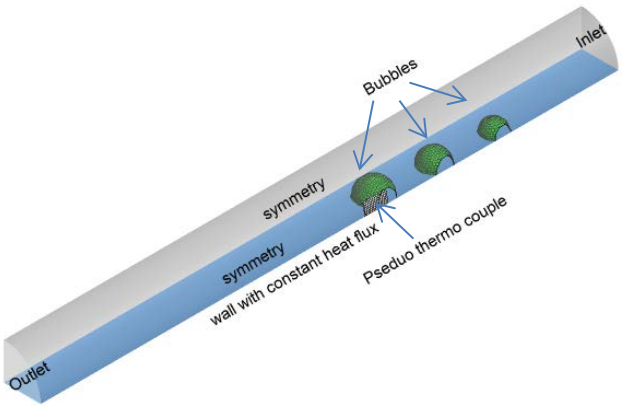

Fig. 1. Simulation domain sketch

2.4 Boundary and initial conditions

A single phase steady laminar simulation is performed and the result is used as the initial condition for the multiphase simulation. Constant heat flux of $10\ kw/m2$ is supplied at the wall. Non-slip velocity boundary condition is applied for the wall. The system operating pressure is 7.0 bar.

Uniform velocity and temperature boundary conditions are used at the inlet at the single phase simulation and the results of this single steady simulation are used as the initial conditions of the multiphase simulation. Some of the settings are list in $Table\ 1$.

Table 1

boundary and initial conditions	Saturated	Subcooled
Presure (bar)	7	
Saturation Temperature (K)	305.15	
Fluid	R 134a	
Initial bubble radius (mm)	0.1/0.12/0.14	
Heat flux (kw/m2)	10	
Mass flux kg/m2*s	335	
Re	1097	
Sub –cooled (K)	0	1

Since Renolyds number is much smaller than 2100, it is clear that inertia force is neglegible

For laminar flow in tubes, there is a thermal entry length where temperature profile is developing along the flow direction. At a certain point the temperature profile has fully developed and the region after this is called fully developed flow. This length is different for different boundary conditions. The one with constant heat flux boundary condition can be calculated by Siegel(Siegel, Sparrow et al. 1958)'s equation:

$$\frac{L_e}{D} = 0.05Re * Pr \qquad (14)$$

In this paper, the thermal entry lengths for given inlet velocity is $34D$ but the length of

the whole simulation domain is shorter than $10D$, which means the studied part of the tube completely falls within the thermal entry region. As it is shown in $Fig\ 4$, The resulting wall temperature is from 3 to 10 K above saturation depending on the position along the tube. An embryo bubble has a 'critical radius' for growth. Bubbles smaller than that will condense and bigger ones will grow (Carey 1992). After the single phase simulation, three small spherical gas bubbles with diameter 0.1, 0.12, and 0.14 mm are then assumed to be present at the tube wall.

The saturation temperature at this pressure is 305.15 K. The temperature and pressure in the bubbles is set to be the saturation temperature and pressure, respectively.

3 Verification and validation

3.1 Mesh independence

In order to check that the calculation is independent of mesh, three cases with different mesh size have been studied. The minimum mesh sizes are $i)\frac{D}{64}, iii)\frac{D}{128}, and\ \ iii)\frac{D}{256}$ respectively. As the $(Fig.2)$ indicates, the bubble growth convergence for the last two mesh sizes. In order to save computational time, a minimum mesh size with $\frac{D}{128}$ is chosen.

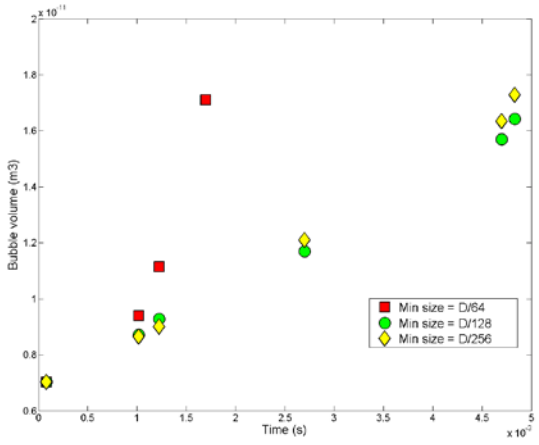

Fig 2. Bubble growth with different mesh sizes

Validation

Visualization comparison

The sliding and merging process of bubbles in micro channels had been recorded by Owhaib. Bubbles generated from nucleate boiling sites close to the inner wall. Due to evaporation, bubbles slides along the channel and absorb heat during this period. When a bubble grows to a certain size, it would departure from the wall and merger with another bubble due to the small diameter of the tube.

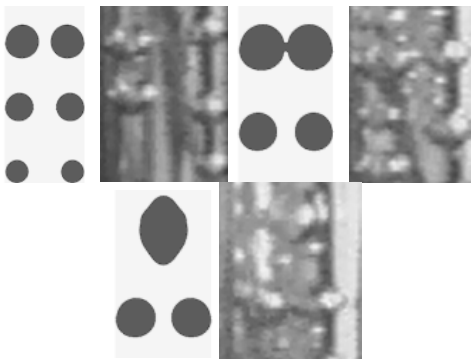

$Fig.$ 3. Simulation and Experimental visualization of flow boiling (Owhaib 2009)
$q = 5\ kW/m2\ ,\ \dot{m} = 90\frac{kg}{m^2} * s$

Heat transfer coefficient

In order to validate the heat transfer, a heat transfer coefficient has to be defined. As mentioned before, a pseudo thermo couple is put at the wall at location $z = [2.0, 2.2]mm$. The area-averaged temperature of this area is measured at every simulation time step. As it shown at Fig 4 , this value become less fluctuated from time $t = 1.0\ ms$. At time 2.0 ms the second bubble pass by this point and time $t = 4.0\ ms$ the third bubble. Therefore the period $t = [2.0, 4.0]ms$ is recorded as a complete period which can be used for heat transfer coefficient calculation.

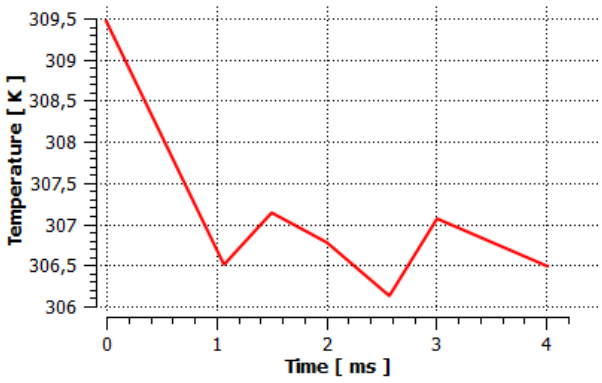

Fig. 4. Pseduo thermocouple temperature

The heat transfer coefficient is defined as

$$h(z) = \frac{q_w}{T_{w,th} - T_f(Z)} \qquad (15)$$

Where $T_{w,th}$is the area-averaged wall temperature of the pseudo thermo couple which locates at $= [2.0, 2.2]mm$, and $T_f(Z)$ is the bulk fluid temperature with the same Z location, is defined as follows

$$T_f(Z) = \frac{\int_{z=2}^{z=2.2} T * u_{m,z}}{\int_{z=2}^{z=2.2} u_{m,z}} \qquad (16)$$

The comparison of the simulation value, experimental results and analytical solution of single phase flow is plotted in fig. When the second bubble or third is passing by the pseudo thermo couple ($t = [2.0, 2.6]$ and $t = [3.5, 4.0]msms$), the heat transfer coefficient is greater than the experimental value, and when there is no bubble passing by, the value is smaller. However, considering the responding time of a real thermo couple under experimental condition, the experimental result should be considered as a time-averaged value which is quite close to the simulated results in this paper.

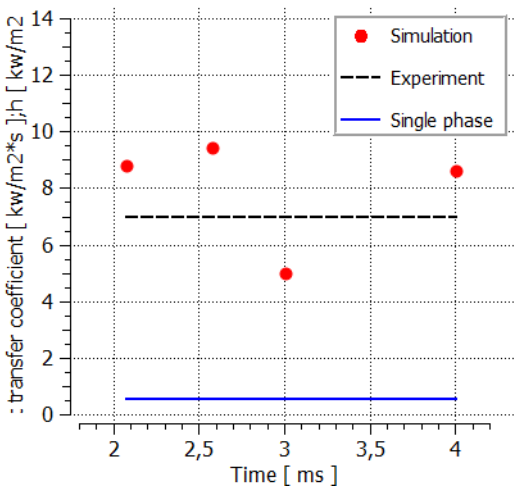

Fig. 5. Heat transfer coefficient validation (Owhaib 2009)
$q = 10\ kW/m2\ ,\ \dot{m} = 335 \frac{kg}{m^2} * s$

4 Results and discussion

Fig. 6 indicates that the bubbles move with different velocity under saturated or sub-cooled inlet condition, even though the sub-cooled degree is very small – only one Kelvin. Under saturated inlet condition, bubbles grow faster than its sub-cooled counterpart. The first pair departs from the wall at around 2.5 ms and starts merger with each other. Sub-cooled flow gives bubbles slower growth rate, they cannot grow big enough to depart from the wall during the whole simulation period.

The bubble growth differs significantly among these two conditions. As shown in fig 7. Saturated inlet condition leads to a much higher growth rate while the sub-cooled one has a very small growth at the beginning and then almost no growth.

This is mainly due to the spatial distribution of evaporation. Since the evaporation is a temperature-controlled process and most of super-heated fluid flow through a relatively thin region close to the inner wall, the most evaporation occurs in this region. Most part of the bubble has a very low evaporation rate, and, under sub-cooled condition, even has a minus evaporation rate-condensation. Since

this condensation region is much bigger than the evaporation one in terms of active area, the total condensation is considerable.

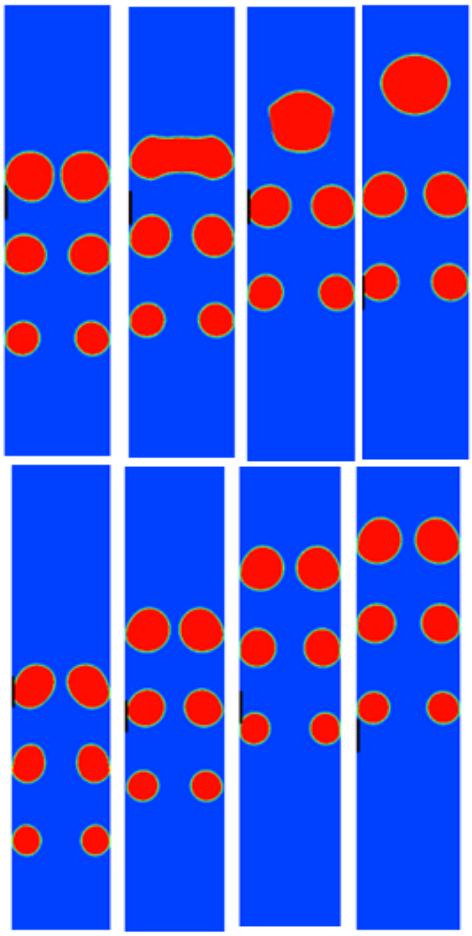

Fig. 6. Bubbles movement at Saturated(Top) and Subcooled(Bottom)conditions

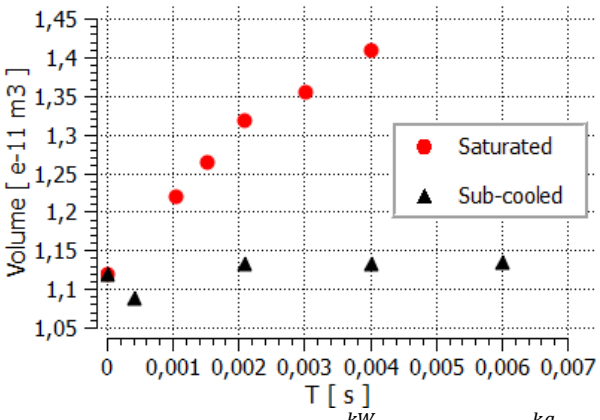

Fig. 7. Bubble growth $q = 10 \frac{kW}{m^2} * s, \dot{m} = 335 \frac{kg}{m^2} * s$

In order to compare the evaporation heat of these two inlet condition quantitatively, an evaporation heat is proposed and defined as

$$q_e = q_{ev} + q_{co} \qquad (17)$$

Where q_{ev} is the total heat for evaporation and q_{co} is for condensation. q_{co} has a negative value. It can be draw from fig that the evaporation heat of saturated boiling is significantly greater than that of sub-cooled. Considering the figure is a logarithm plot, the heat for phase change in sub-cooled boiling can be neglected. The input heat from the wall is smaller than then saturated evaporation heat, but still much higher than the sub-cooled one.

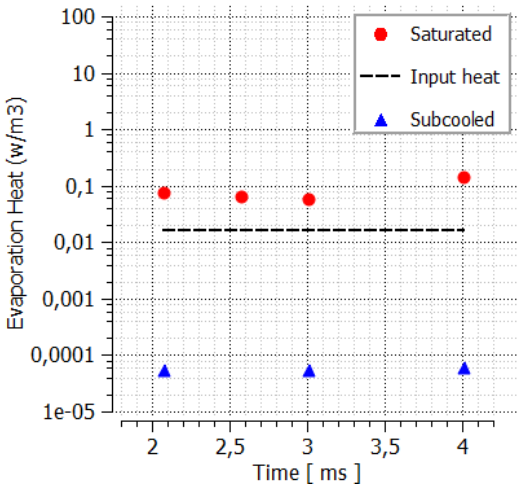

Fig .8 Evaporation heat $\left(\frac{w}{m3}\right)$

On the other hand, the heat transfer coefficient, which plot in *Fig* .10, tells a different story. The saturated one is still higher than its sub-cooled counterpart, but with a much small margin. The reason behind this is that the heat transfer mechanism difference. In the saturated boiling, heat transfer through the evaporation at the interface. But in the sub-cooled boiling, the heat transfer process is more complicated and involves a bigger region. First, the heat transfer from the boundary layer to the bubble by evaporation. Then, there is a heat conduction or even micro convection inside the bubble which make the whole bubble at a homogenous temperature-the saturated

temperature. Lastly, the condensation transfers the heat from bubble to the liquid surrounding.

The cross section of temperature profile drawn in *Fig.* 9 indicates these process, bubbles distort the thermo boundary layer therefore reduce wall temperature and enhance heat transfer. In the sub-cooled case, evaporation and condensation both plays an interesting role in heat transfer. Bubbles receive heat from the thermal boundary layer and evaporate, and, on the other side, they also condense at the center of channels, which release heat to the liquid.

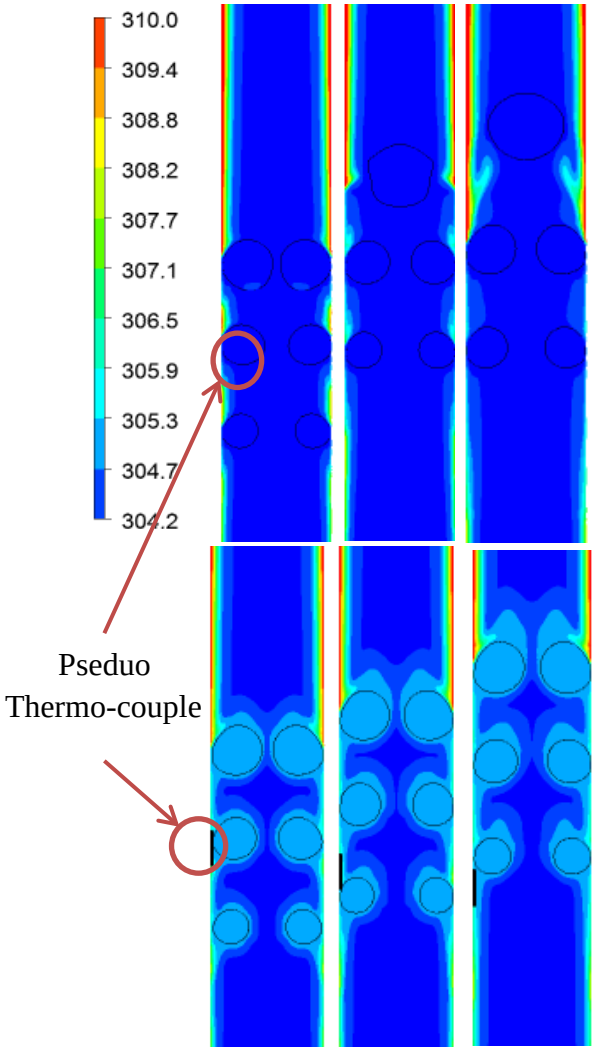

Fig. 9. *Temperature contour under Saturated(Top) and Subcooled(Bottom) conditions* $t = 2, 3, 4\ ms$

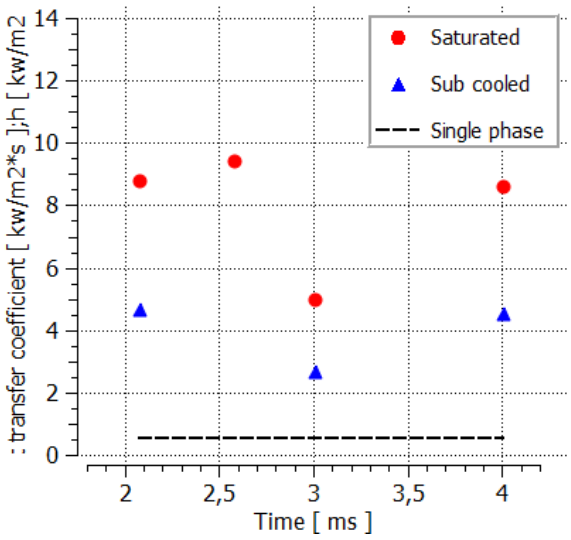

Fig. 10. *Heat transfer coefficient*

5 Conclusion

A three dimensional numerical study on the transition of convective boiling from nucleate boiling to bubbly flow in a micro-channel with diameter of 0.64 mm have been done. It is found that the growing and merging of bubbles affect the heat transfer significantly. The heat transfer under saturated and sub-cooled conditions differs each. The following conclusions can be drawn based on the study:

1 The growth of bubbles in micro-channels during saturated and sub-cooled flow boiling has been successfully simulated. Both visualization and heat transfer coefficient have good agreements with the experimental results. The bubbles will merge with each other during saturated boiling after depart from the wall. On the contrary, the merge is not happened under the sub-cooled condition due to a much lower bubble growth.

2 Bubbles have much higher evaporation rate during saturated flow boiling than sub-cooled one. The evaporation heat is higher than the input heat under saturated flow boiling and magnitude lower under sub-cooled condition. However, the heat transfer coefficient of saturated boiling is only slightly higher than its sub-cooled counterpart.

3 Heat transfer enhancement in saturated flow boiling is mainly due to evaporation therefore is simply a temperature controlled process. On the other hand, the sub-cooled one has a more complicated mechanism. The effects of sub cool degree, heat flux and mass flux may play an important role and need to be further studied.

Nomenclature list

Latin letters

A *area* (m^2)
C *accommodation coefficient*
c *specific heat*
D *diameter*
Eo *Etovos number*
F *force*
H *heat*
L *length*
P *pressure*
Pr *prandlt number*
q *heat flux*
k *heat conduction coefficient*
Rg *gas constant*
Re *reynolds number*
T *temperature*
u *velocity*
$u_{m,Nfz}$ *local mass velocity* kg/s
We *Weber number*
Z *vetical distance* (m)
$\boldsymbol{n}$ *normal vector*

Greek letters

α *Volume fraction*
β *bubble growth constant*
σ *surface tension*
ρ *density*
μ *viscosity*
$\emptyset$ *level set function*

Subscript

c *condensation*
e *evaporation*
f *fluid*
l *liquid*
gr *grid*
int *interface*
o *operating*
v *vapor*
w *wall*
sat *saturation*

References

Agostini, B., R. Revellin, et al. (2008). "Elongated bubbles in microchannels. Part I: Experimental study and modeling of elongated bubble velocity." International Journal of Multiphase Flow 34(6): 590-601.

Carey, V. P. (1992). Liquid-vapor phase-change phenomena.

Hardt, S. and F. Wondra (2008). "Evaporation model for interfacial flows based on a continuum-field representation of the source terms." Journal of Computational Physics 227(11): 5871-5895.

Liu, Q., B. Palm, et al. (2012). Simulation on the flow and heat transfer characteristics of confined bubbles in micro-channels. ASME 2012 10th International Conference on Nanochannels, Microchannels, and Minichannels collocated with the ASME 2012 Heat Transfer Summer Conference and the ASME 2012 Fluids Engineering Division Summer Meeting, American Society of Mechanical Engineers.

Magnini, M., B. Pulvirenti, et al. (2013). "Numerical investigation of hydrodynamics and heat transfer of elongated bubbles during flow boiling in a microchannel." International Journal of Heat and Mass Transfer 59(0): 451-471.

Mukherjee, A. and S. G. Kandlikar (2005). "Numerical simulation of growth of a vapor bubble during flow boiling of water in a microchannel." Microfluidics and Nanofluidics 1(2): 137-145.

Owhaib, P. (2009). "Experimental Heat Transfer, Pressure Drop, and Flow Visualization of R 134a in Vertical MiniMicro Tubes." PhD Thesis.

Revellin, R., B. Agostini, et al. (2008). "Elongated bubbles in microchannels. Part II: Experimental study and modeling of bubble collisions." International Journal of Multiphase Flow 34(6): 602-613.

Siegel, R., E. Sparrow, et al. (1958). "Steady laminar heat transfer in a circular tube with prescribed wall heat flux." Applied Scientific Research, Section A 7(5): 386-392.

Thome, J. R. and Collier (1994). "Flow boiling in a uniformly heated circular tube."